

Article

# Raman and Photoemission Spectroscopic Analyses of Explanted BioloX<sup>®</sup> Delta Femoral Heads Showing Metal Transfer

Paola Taddei <sup>1,\*</sup> , Eleonora Pavoni <sup>1</sup> and Saverio Affatato <sup>2</sup> 

<sup>1</sup> Dipartimento di Scienze Biomediche e Neuromotorie, Università di Bologna, Via Belmeloro 8/2, 40126 Bologna, Italy; eleonora.pavoni2@unibo.it

<sup>2</sup> Laboratorio di Tecnologia Medica, Istituto Ortopedico Rizzoli, Via di Barbiano, 1/10, 40136 Bologna, Italy; affatato@tecno.ior.it

\* Correspondence: paola.taddei@unibo.it; Tel.: +39-051-2094280

Received: 28 April 2017; Accepted: 29 June 2017; Published: 3 July 2017

**Abstract:** BioloX<sup>®</sup> delta has been widely used in joint replacements thanks to its high strength and wear resistance. In this study, eleven BioloX<sup>®</sup> delta femoral head retrievals affected by metal transfer (MT) were analysed by Raman spectroscopy to estimate the tetragonal to monoclinic zirconia phase transformation, whose occurrence may compromise ceramic chemical stability and mechanical strength. The residual stress state was evaluated by both Raman and photoemission spectroscopy.  $V_m$  monoclinic zirconia contents were higher near the centre of the articulating surface and in the MT area than in the border control area of the retrievals. In only one retrieval, stress related to MT appeared a more severe condition, able to induce zirconia phase transformation; for all the others, stresses related to loading in the central region and related to MT, were conducive to a zirconia phase transformation of nearly the same extent.  $V_m$  depth profiling analyses showed that the transformation involved different thicknesses in different samples. Raman data allowed for the investigation of the mechanism of zirconia phase transformation and confirmed that the growth stage was absent and the nucleation stage was not occurring as freely as it would in unconstrained zirconia.

**Keywords:** BioloX<sup>®</sup> delta; retrievals; hip joint prostheses; femoral heads; wear; metal transfer; zirconia phase transformation; Raman spectroscopy; photoemission spectroscopy

## 1. Introduction

BioloX<sup>®</sup> delta is a zirconia toughened alumina (ZTA) commercial product developed by CeramTec AG (Germany) for biomedical applications. More in detail, BioloX<sup>®</sup> delta is made of yttria-stabilized tetragonal zirconia particles (Y-TZP) homogeneously dispersed into an alumina matrix [1]: the alumina content is about 75% in weight with an average grain size around 0.54  $\mu\text{m}$ , while the Y-TZP content is about 24% by weight, with an average grain size around 0.27  $\mu\text{m}$ . BioloX<sup>®</sup> delta composite also contains 1% of  $\text{Cr}_2\text{O}_3$ , together with less abundant compounds, such as SrO [1].

Alumina is chemically stable and confers hardness and wear resistance to the material, while Y-TZP particles are included into the formulation to improve its mechanical properties; indeed, they produce local pressure peaks in the area of cracks, counteracting their propagation.

Besides this strengthening mechanism (common to all ZTA ceramics), BioloX<sup>®</sup> delta has another active characteristic. In fact, SrO forms platelet-like crystals that prevent crack initiation and propagation by deflecting the crack path and neutralizing its energy, thereby increasing the strength and toughness of the material. On the other hand,  $\text{Cr}_2\text{O}_3$  is included into the formulation to counterbalance the reduction of hardness caused by the introduction of zirconia, although the actual impact of  $\text{Cr}_2\text{O}_3$  on hardness in BioloX<sup>®</sup> delta is still under discussion [2,3].

Biolox<sup>®</sup> delta ceramic is currently used to manufacture prosthetic components for joint replacement (i.e., hip, knee, shoulder) and offers excellent performances thanks to its high strength, wear resistance and stability, nontoxicity, and biocompatibility in vivo [4–6]. However, recent studies have demonstrated the presence of a close relation between stress and the tetragonal to monoclinic zirconia phase transformation, which may compromise ceramic mechanical strength [7,8] and chemical stability [9,10]. Moreover, this transformation involves a volume expansion (3–4%) that induces additional compressive stresses [11–16].

The occurrence of tetragonal to monoclinic zirconia transformation in Biolox<sup>®</sup> delta is not the only unfavourable aspect; an additional one (also common to other ceramic materials) concerns metal transfer (MT), which may alter the bearing surface (e.g., due to head dislocation, closed reduction procedures, impingement, or third-body wear particle entrapment in the articulating zone [17]), and could have detrimental effects on wear [18].

MT has a dark and metallic colour and may consist of titanium (Ti) or cobalt-chromium (CoCr) alloy and has been shown to increase the surface roughness of ceramic femoral heads [19,20]. MT can occur in different phases:

- through intraoperative reduction of total hip arthroplasty (THA) if the ceramic head comes into contact with the acetabular rim [21];
- during primary THA if there are any intraoperative difficulties in reduction or if multiple dislocation/relocation manoeuvres are necessary during surgery [19];
- after surgery [15].

The present study was aimed at investigating a series of Biolox<sup>®</sup> delta femoral head retrievals in order to estimate tetragonal to monoclinic zirconia phase transformation by Raman spectroscopy and to evaluate residual stress state by using both Raman and photoemission spectroscopy.

Retrievals were analysed in their border (control area), at the centre of the articulating surface (i.e., the most worn area) and near the MT region, in order to assess if MT related stress may aggravate zirconia phase transformation.

Raman spectroscopy appeared a valid method to evaluate tetragonal to monoclinic zirconia phase transformation, thanks to the characteristic Raman bands assigned to the two polymorphs, whose intensity is proportional to their concentration, thus allowing to calculate the zirconia monoclinic phase volume fraction [13,22–24].

The residual stress state of the material was assessed by exploiting its piezospectroscopic effect, which causes a shift of the spectral bands (Raman, IR or photoemission bands) in response to an applied strain or stress [25–30]; in the present study, the changes induced by stress in the wavenumber position and width of the Raman bands of zirconia, as well as of the photoemission bands ( $R_1$  and  $R_2$ ) due to  $Cr^{3+}$  [25,26] have been investigated.

## 2. Materials and Methods

### 2.1. Materials

Ceramic femoral heads were explanted during revision arthroplasty at Rizzoli Orthopaedic Institute (Bologna, Italy) and catalogued in a Register of Orthopaedic Prosthetic Explants (REPO). Eleven Biolox<sup>®</sup> delta femoral heads removed from 11 patients after different periods (ranging between 0.1 and 5.4 years), were selected as affected by the MT phenomenon.

The femoral heads were cleaned by submersion in an enzymatic detergent and wiped with acetone before being observed.

All patients had undergone a primary THA at our hospital between 2006 and 2011, comprising of four women and seven men, and they were aged between 48 and 82 years at revision. In most cases, the reason for failure was aseptic loosening of the acetabular component.

More details are shown in Table 1.

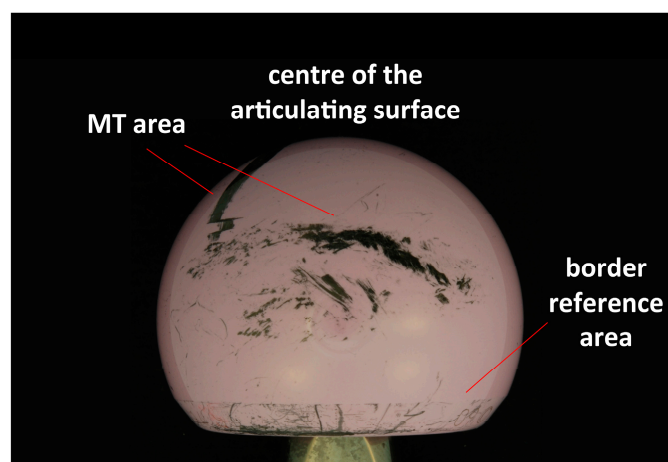
**Table 1.** Details on the BioloX<sup>®</sup> delta retrievals under study (head surface area, MT area, and MT rate % data from [31]).

Head Number	Age at Surgery	Follow-Up (yr)	Gender	Implant Side	Implantation Year	Head Surface Area (mm <sup>2</sup> )	MT Area (mm <sup>2</sup> )	MT Rate %
#1	69	3.7	M	right	2006	3392.9	85.8	2.5
#2	62	2.4	F	right	2008	2824.9	95.3	3.4
#3	68	5.4	F	right	2008	3392.9	127.9	3.8
#4	56	0.1	M	right	2009	2804.8	286.1	10.2
#5	61	0.2	F	right	2010	2804.8	160.9	5.7
#6	82	0.1	M	left	2010	2804.8	71.9	2.6
#7	76	0.2	F	left	2010	2764.6	95.1	3.4
#8	77	0.1	M	right	2010	2804.8	126.5	4.5
#9	48	0.2	M	right	2010	2804.8	33.1	1.2
#10	68	0.5	M	right	2011	2804.8	33.0	1.2
#11	56	1.9	M	left	2011	3415.5	234.5	6.9

## 2.2. Micro-Raman and Photoemission Spectroscopy

Micro-Raman spectra were obtained using a Jasco NRS-2000C instrument (Easton, MD, USA) in back-scattering conditions with 4 cm<sup>-1</sup> spectral resolution, using the 532 nm Green Diode Pumped Solid State (DPSS) Laser Driver (RgBLase LLC, Fremont, CA, USA) with a power of ca. 25 mW, properly filtered. A 160 K cooled digital CCD (Spec-10: 100B, Roper Scientific Inc., Trenton, NJ, USA) was used as a detector. The spectra were recorded under different conditions: (a) using a 10× magnification microscope; (b) using a 100× magnification microscope with a confocal pinhole with an aperture diameter of 3000 μm; and (c) using a 100× magnification microscope with a confocal pinhole with an aperture diameter of 200 μm. The optical conditions (a) were used for comparison, since they were the same used in our previous studies [13,14]. The other optical conditions were chosen to obtain signals from a more limited in-depth region (with field depths of about 20 and 10 μm, respectively, according to previous studies [32]), and, thus, to gain information on the samples surface.

Retrievals were analysed in different areas: near the centre of the articulating surface (i.e., the most worn area), on the border of each head (which was taken as reference) and in the MT area (Figure 1); at least ten spectra were recorded in each region under each of the optical conditions specified above. In the border region, areas free from scratches and metal staining were chosen.

**Figure 1.** Areas of the femoral head where the spectra were taken.

The zirconia monoclinic phase volume fraction ( $V_m$ ) was evaluated according to Katagiri et al. [22] using the following equation:

$$V_m = \frac{I_m^{183} + I_m^{191}}{2.2 \times I_t^{148} + I_m^{183} + I_m^{191}} \quad (1)$$

where  $I_m^{183} + I_m^{191}$  and  $I_t^{148}$  were the areas of the monoclinic doublet at about 183 and 191  $\text{cm}^{-1}$  and the tetragonal band at 148  $\text{cm}^{-1}$ , respectively.

Selected femoral heads were further analysed in the former area by recording the micro-Raman spectra ( $100\times$  magnification, pinhole 200  $\mu\text{m}$ ) at increasing depth below the bearing surface in three to five different points. Femoral heads #1, #2, #5, #7, #9, #10, and #11 were chosen since they showed a significant  $V_m$  increase in their MT areas compared to the border control region under optical conditions (b). Femoral head #3 was analysed due to its follow-up time, which was the highest among the retrievals under study.

All the femoral heads were analysed by photoemission spectroscopy. Spectra were recorded in back-scattering conditions with 0.5  $\text{cm}^{-1}$  spectral resolution using the above mentioned instrument, laser and detector. Spectra were recorded using optical conditions (a), (b), and (c), as described above, in the same sample regions (at least ten spectra for each region). To ensure that no laser heating occurred, all measurements were performed at a low laser power (i.e., 1 mW). Instrumental fluctuations represent another source of possible variation in the measured frequency. In order to correct for this, a characteristic neon line at 14,431  $\text{cm}^{-1}$  was used as a frequency calibration standard. The bands monitored were at about 14,397  $\text{cm}^{-1}$  ( $R_1$ ) and 14,427  $\text{cm}^{-1}$  ( $R_2$ ), assignable to the radiative electronic transitions of the  $\text{Cr}^{3+}$  ions present in  $\text{Cr}_2\text{O}_3$  as well as in the  $\text{Al}_2\text{O}_3$  lattice as substitutional impurities. Width (expressed as full width at half maximum, FWHM), intensity and wavenumber of  $R_1$  and  $R_2$  bands were determined by fitting the experimental spectra with mixtures of Lorentzian and Gaussian functions. Fitting was done using a commercial software (OPUS 6.5, Bruker Optik GmbH, Ettlingen, Germany).

All Raman and photoluminescence measurements were made in a fully non-destructive manner, without any sample manipulation.

### 2.3. Statistical Analysis

Photoemission and Raman data have non-Gaussian distributions. Therefore, we used a non-parametric test. A non-parametric Kruskal-Wallis test was used to measure statistical significance (set at  $p < 0.05$ ) and a Dunn-Bonferroni post-hoc analysis was performed for any dependent variable for which the Kruskal-Wallis test was significant.

## 3. Results

### 3.1. Photoemission Spectroscopy

A representative emission spectrum of a BioloX<sup>®</sup> delta femoral head fitted into the two  $R_1$  and  $R_2$  components is shown in Figure 2.

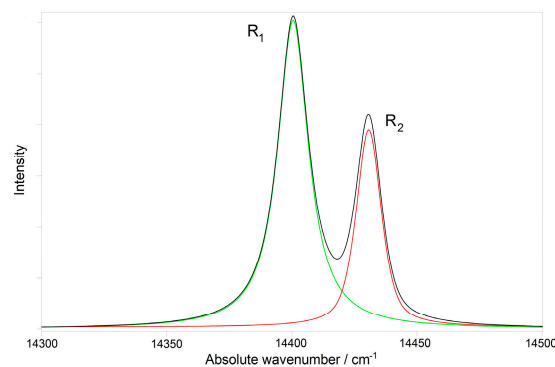


**Figure 2.** Representative photoemission spectrum of a BioloX<sup>®</sup> delta femoral head fitted into the  $R_1$  and  $R_2$  components.

At room temperature,  $R_1$  and  $R_2$  bands are positioned at about 14,397 and 14,427  $\text{cm}^{-1}$  (generally with a  $\Delta E (R_2 - R_1) \approx 30 \text{ cm}^{-1}$ ) indicating a ruby like high-field crystalline environment that causes a spin-forbidden transition ( ${}^2E \rightarrow {}^4A_2$ ) [33,34].

As shown in Figure 3 and Figure S1, Supplementary Material,  $R_1$  and  $R_2$  FWHM values measured under optical conditions (b) were mostly coincident with those recorded under optical conditions (c), but significantly lower (in most samples) compared to those obtained under optical conditions (a).

FWHM values of both  $R_1$  and  $R_2$  bands measured in the unworn control areas of the retrievals (Figure 3) showed a generally decreasing trend as a function of the implantation year, although high batch-to-batch variations were detected, as it can be seen in Figure S2a,b, Supplementary Material.

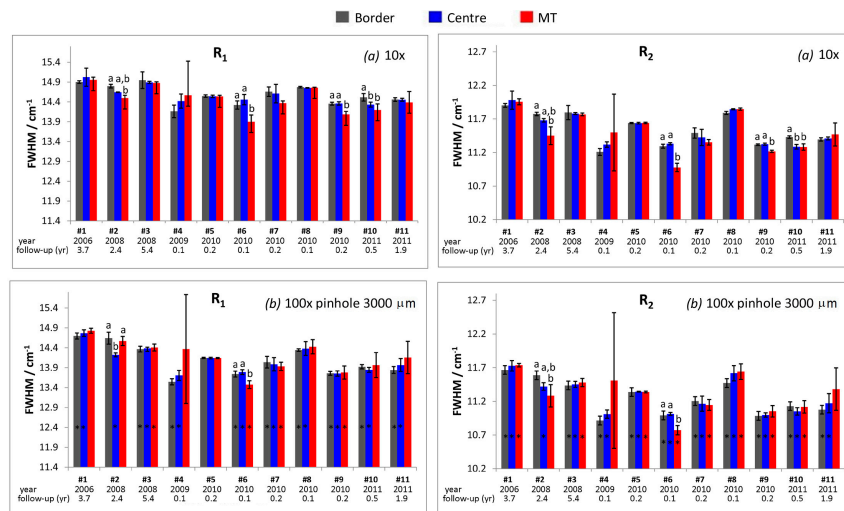


**Figure 3.** The average FWHM values ( $\text{FWHM} \pm \text{standard deviation}$ ) of the  $R_1$  and  $R_2$  bands as obtained from the fitting of the emission spectra recorded under optical conditions (a) and (b) in different areas of the explanted BioloX<sup>®</sup> delta femoral heads. When present, different letters on the histogram bars indicate significant differences among the areas of each retrieval; asterisks indicate significant differences between the values measured under optical conditions (a) and (b) within the same area and in the same retrieval.

In any of the retrievals, no significant differences among the different areas (i.e., border control area, centre, and MT area) were observed regarding wavenumber position or intensity of the  $R_1$  and  $R_2$  bands.

Conversely, significant changes in FWHM were observed in femoral heads #2, #6, #9, and #10 (Figure 3). For retrieval #2, the  $R_2$  FWHM value measured in the MT area was lower than the one of the border and the same trend was observed for the  $R_1$  band under optical conditions (a). For retrievals #6 and #9, FWHM values measured in the MT area were lower than those measured both in the centre and border areas, while in sample #10, they were lower only than those of the border. No significant FWHM changes were detected in the MT area of femoral head #4, due to the high standard deviation associated to the measurements. However, local FWHM increases were observed in some single spectra, attaining values as high as 14.1 and 17.9  $\text{cm}^{-1}$  for  $R_1$  and  $R_2$  bands, respectively.

Spectral changes did not appear related to the follow-up time; in fact, the sample with the highest follow-up (i.e., #3) did not undergo any significant change in the FWHM of the emission bands, and the samples that showed the most significant changes were characterized by significantly lower follow-up times (ranging between 0.1 and 2.4 years).

### 3.2. Micro-Raman Spectroscopy

As an example, Figure 4 shows the average micro-Raman spectra recorded under the optical conditions (a) and (b) in the different regions of BioloX<sup>®</sup> delta femoral head #11.

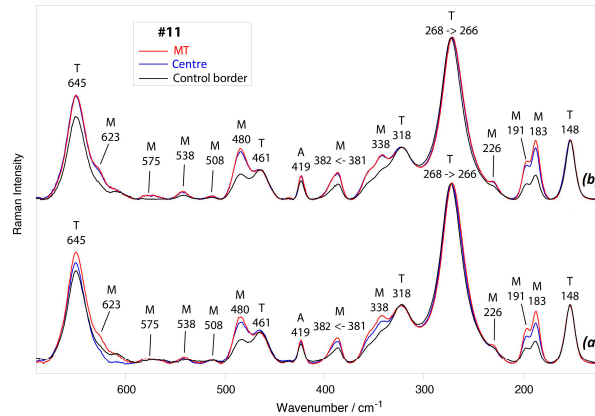


**Figure 4.** Average micro-Raman spectra recorded under optical conditions (a) and (b) in the border control area (black), near the centre of the articulating surface (blue), and in the MT area (red) of BioloX<sup>®</sup> delta retrieval #11. The bands assignable to alumina (A), tetragonal (T), and monoclinic (M) zirconia are indicated.

As already observed for photoemission measurements, spectra measured under optical conditions (c) were practically coincident with those recorded under the optical conditions (b) and, thus, are not reported.

Spectra reported in Figure 4 showed, with different relative intensities, the bands of tetragonal zirconia (at about 645, 461, 318, 268, and 148  $\text{cm}^{-1}$ ) and monoclinic zirconia (at 623, 575, 538, 508, 480, 381, 338, 226, and 191–183  $\text{cm}^{-1}$ ) [35,36]; moreover, the band at 419  $\text{cm}^{-1}$ , belonging to alumina [37], was detected.

In the spectra recorded near the centre of the articulating surface and in the MT area of femoral head #11, under all optical conditions, the relative intensity of the marker bands of monoclinic zirconia appeared higher than in those recorded in the border control area, suggesting that in the former two areas the monoclinic content was higher than in the latter. This qualitative result was confirmed by quantitative  $V_m$  values obtained under optical conditions (a) and (b) on the retrievals under study (Figure 5).

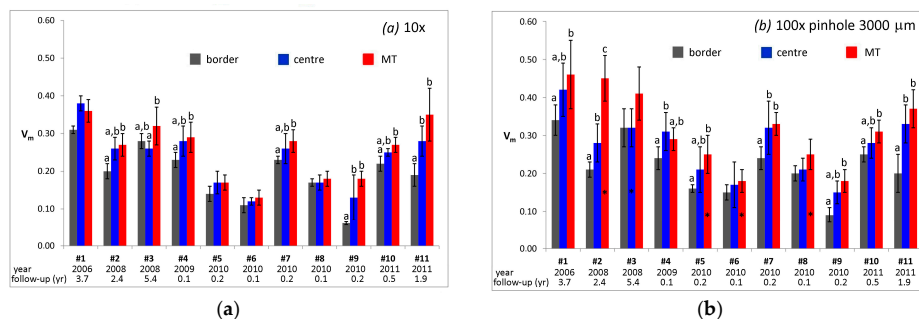


**Figure 5.** Average  $V_m$  values calculated from the micro-Raman spectra recorded under optical conditions (a) (a) and (b) (b), in different areas of the explanted BioloX<sup>®</sup> delta femoral heads. When present, different letters on the histogram bars indicate significant differences among the areas of each retrieval; asterisks indicate significant differences between the values measured under optical conditions (a) and (b) within the same area and in the same retrieval.

As shown in Figure 5, in retrieval #11, the MT area and the centre of the articulating surface were characterized by not significantly different  $V_m$  values, but significantly higher than the border control region resembling the trend of the spectra reported in Figure 4. The same trend was also observed for retrievals #7 and #9; for retrieval #4, the differences among the areas depended on the optical conditions. For retrievals #1, #5, and #10, significant differences were observed only between the MT area and the control border. Retrieval #2 was the only one showing significant differences among all the three areas, using optical conditions (b) and (c).

As previously observed for photoemission measurements,  $V_m$  changes were not found to be related to the follow-up time, as may be easily observed from Figure S3, Supplementary Material: samples showing the most significant %  $V_m$  increases in the centre and MT areas were not those characterised by the highest follow-up times. In particular, among the above mentioned retrievals, femoral heads #4, #5, #7, #9, and #10 were implanted for less than one year.

With regards to the unworn control areas, it may be observed that their  $V_m$  values underwent a general decrease with the implantation year, as also shown in Figure S2c, Supplementary Material.

Going from optical conditions (a) (Figure 5a) to (b) (Figure 5b), a general increase of  $V_m$  values, as well as in their associated standard deviation, was observed in the centre, and even more in the MT area.

To gain more insights into this aspect,  $V_m$  depth profiling analyses were carried out on some selected femoral heads; Figure 6 reports the trend of  $V_m$  monoclinic content measured in the MT area as a function of depth: each point represents the average value of three to five different measurements carried out in different points of the MT region.

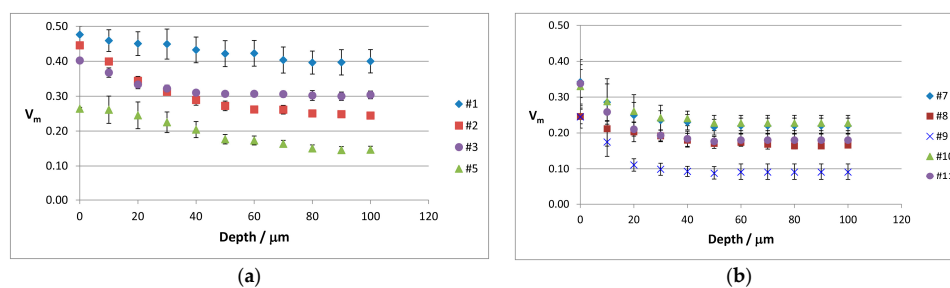


**Figure 6.** The trend of the  $V_m$  monoclinic content as a function of depth in the MT area of femoral heads (a) #1, #2, #3, #5; and (b) #7, #8, #9, #10, and #11. Each point represents the average value of three to five different measurements carried out in different points.

As the distance from the sample surface increased, a decrease in the monoclinic content was observed for all retrievals, although to different rates, as also shown in Figure 7.

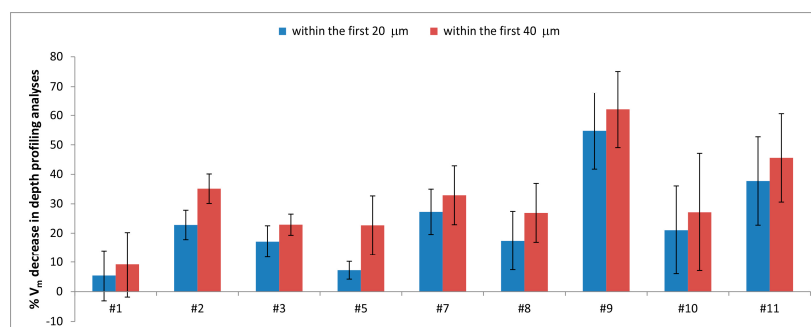


**Figure 7.** %  $V_m$  decrease recorded within the first 20 and 40  $\mu\text{m}$  in depth profiling analyses of femoral heads #1, #2, #3, #5, #7, #8, #9, #10, and #11.

#### 4. Discussion

In this study, eleven Biolox<sup>®</sup> delta femoral heads affected by MT were analysed in different regions, i.e., their border, near the centre of the articulating surface, and in the MT region.

Unfortunately, the measurement of the  $V_m$  value before implantation is not clinically possible and this information has never been reported in previous retrieval studies.

The suitability of the retrievals border as a reliable control area for comparison could be questioned, since the monoclinic zirconia content in this area could be different from that before implantation, due to hydrothermal ageing phenomenon. In fact, it is well known that water alone may trigger zirconia phase transformation, so in vivo permanence could have altered, to a certain extent, the monoclinic content also in the border unworn area of the retrievals. This hypothesis could be rejected on the basis of the  $V_m$  values measured in depth in the samples, i.e., 100  $\mu\text{m}$  below the surface, where hydrothermal ageing and mechanical solicitations able to trigger the zirconia phase transformation should be negligible. As shown in Figure S4, Supplementary Material, for all the analysed retrievals,  $V_m$  values measured 100  $\mu\text{m}$  below the surface were not significantly different compared to those obtained from the border, suggesting that the latter region represents a reliable control area for comparison. This result was obtained also for retrieval #3, which had the highest follow-up among the analysed samples (5.4 years). Our results showed that an in vivo ageing as long as 5.4 years did not alter the zirconia phase distribution in Biolox<sup>®</sup> delta femoral heads. These results are in agreement with the Raman in-depth profiling mapping of Biolox<sup>®</sup> delta retrievals recently reported by Pezzotti et al. [38]: also for their samples, the  $V_m$  content measured 100  $\mu\text{m}$  below the surface was not noticeably different with respect to the average value measured on the sample surface in the control non-wear zone. On the other hand, our finding is in agreement with earlier studies on Biolox<sup>®</sup> delta femoral heads where the authors did not report any significant tetragonal to monoclinic phase transformation after environmental exposure to water vapour [1,39]. Conversely, more recent studies have reported that Biolox<sup>®</sup> delta femoral heads underwent significant phase changes after in vitro accelerated aging tests [40].

FWHM of  $R_1$  and  $R_2$  bands and  $V_m$  values measured in the unworn control areas of retrievals showed a generally decreasing tendency as a function of the implantation year (Figure S2, Supplementary Material, right). The general sharpening of  $R_1$  and  $R_2$  bands may be interpreted as a sign of a sharper distribution of residual stress states. Moreover, from 1999 to 2011 a general decrease of the monoclinic content was observed. Both these behaviours suggest that the manufacturer generally improved the material properties in this time period, confirming our previous findings [13]. However, batch-to-batch variations seem to be present: with regards to the five retrievals dated back to 2010, their  $V_m$  values appeared quite dispersed (Figure 5), ranging between  $0.060 \pm 0.004$  and  $0.023 \pm 0.01$ . This result is in agreement with the study by Bal et al., which has reported a broad range of monoclinic contents also for even more recent components [41].

FWHM values of  $R_1$  and  $R_2$  bands showed significant variation among the unworn control area, the central region and the MT zone of retrievals #2, #6, #9, and #10 (Figure 3); stress related to MT phenomenon and loading in the centre of the articulating surface led to a sharpening of the photoemission bands. However, no significant changes in the wavenumber position of  $R_1$  and  $R_2$  bands were detected. The latter result, although already reported by Grabner [30], as well as in our previous studies [13,42–44], could be surprising, considering that the wavenumber shift of  $R_1$  and  $R_2$  bands has been reported to be more stress sensitive than their width (the stress dependence of these parameters is about 2.46, 2.50  $\text{cm}^{-1}/\text{GPa}$  and less than 1  $\text{cm}^{-1}/\text{GPa}$ , respectively [27,45]). Our result can be explained by considering that stress values reported for alumina in similar alumina–zirconia composites were below 100 MPa [46] and, thus, band shifts appeared undetectable under the used experimental setup. On the other hand, in a polycrystalline material, although the average stress over the material must be zero, variations in stress from one grain to another can cause changes in FWHM values.

The sharpening of  $R_1$  and  $R_2$  bands in the above mentioned samples may be explained through the micro-cracking effect, which causes a reduction of the width of Gaussian residual stress distribution [47]; the same result was obtained for a fractured alumina femoral head tested under severe wear conditions [42]. For retrievals #6 and #9, the MT area showed a sharpening of  $R_1$  and  $R_2$  bands, which was not observed in the centre of the articulating surface (Figure 3), suggesting that only stress related to the MT phenomenon induced micro-cracking in these samples. Conversely, for femoral head #10, both MT and loading in the centre of the articulating surface induced this effect.

Femoral head #4 showed a behaviour different from all the other retrievals; although not significant, FWHM values underwent a certain increase in the MT area. As described by Grabner [30], the broadening of photoemission bands could be seen as a variation in the distribution of the residual stress states; in particular, the micro-stress could vary from one crystallite to another, causing a broadening of the bands. Moreover, in polycrystalline materials the variations in stress, from one grain to another, cause a widening of the photoemission bands due to the superposition of features originated from individual photoemitter volumes [26].

The average micro-Raman spectra reported in Figure 4 showed that both tetragonal and monoclinic phases underwent compressive stresses following implantation, in agreement with the results reported by a recent study on in vivo worn retrievals [48]. In fact, going from the control border to the centre and MT areas of sample #11, the bands at  $268\text{ cm}^{-1}$  (tetragonal zirconia) and  $381\text{ cm}^{-1}$  (monoclinic zirconia) shifted to  $266$  and  $382\text{ cm}^{-1}$ , respectively, i.e., to opposite directions. A similar behaviour, already detected in our previously analysed BioloX<sup>®</sup> delta and zirconia retrievals [13,15,16], is not surprising since the band at  $381\text{ cm}^{-1}$  has a negative piezospectroscopic coefficient, while for the band at  $268\text{ cm}^{-1}$  the piezospectroscopic coefficient is positive [49].

Raman spectroscopy plays an important role in determining the monoclinic zirconia content in BioloX<sup>®</sup> delta; the  $V_m$  parameter results of primary importance because it is well known that the tetragonal to monoclinic transition may compromise the mechanical strength of the material [7,8] and its long-term lifetime and stability [9,10].

Figure 5 showed significant differences between  $V_m$  values calculated in the border control area and in the centre of the articulating surface in retrievals #2, #4, #7, #9, and #11, confirming that the centre of the articulating surface may undergo significant  $V_m$  increases upon stress, related to the service [13]. Similarly, significant differences were found between  $V_m$  values obtained in the border and MT areas in retrievals #1, #2, #4, #5, #7, #9, #10, and #11. Only for femoral head #2, the  $V_m$  value measured in the MT area was significantly higher than the one measured in the central area and both these contents were higher than in the border. Therefore, only for this retrieval, stress related to MT appeared a more severe condition able to induce zirconia phase transformation. For all the other retrievals, stresses related to loading in the central region and to MT phenomenon in the corresponding area were conducive to a zirconia phase transformation of nearly the same extent; in other words, for most retrievals, the two stress conditions did not appear significantly different with regards to the above mentioned transformation, as observed for previously-analysed zirconia retrievals [15]. From the graphs reported in Figure S3, Supplementary Material, it appears clear that  $V_m$  increases observed in the centre and MT areas were not related to the follow-up time, in agreement with Parkes et al. [50]. Among the retrievals that showed the most significant increases, some had been implanted for less than one year (#4, #5, #7, #9, #10). Such an unexpected transformation was observed also by Zhu et al., in short-term retrieved BioloX<sup>®</sup> delta-on-metal hip implants [51]. These authors have suggested that frictionally-driven metal transfer to the ceramic lattice destabilizes the chemistry of its surface and results in abnormally high  $V_m$  values in short-term retrievals. This phenomenon may also explain the results obtained in the present study on the MT-affected BioloX<sup>®</sup> delta femoral heads.

Data reported in Figure 5 showed that  $V_m$  values depend on the optical conditions used, especially in the MT area of the retrievals.  $V_m$  depth profiling analyses (Figure 6) carried out in the MT area allowed to clarify that the phase transformation involved different depths in different samples. As shown in Figure 7, retrievals #1 and #5 showed the lowest %  $V_m$  decrease within the first  $20\text{ }\mu\text{m}$

of sample depth. However, for the former the %  $V_m$  decrease in the first 40  $\mu\text{m}$  of sample depth was comparable, while for the latter it was significantly higher, as observed also for retrieval #2. This trend would suggest that in femoral head #1, no further  $V_m$  decrease occurred between 20 and 40  $\mu\text{m}$ , as also observable in Figure 6a; in other words, at a 40  $\mu\text{m}$  depth the material has already attained a  $V_m$  value not significantly different from that measured in border control area. Conversely, for retrievals #2 and #5,  $V_m$  continued to also decrease below 40  $\mu\text{m}$  (as also shown in Figure 6a), and the  $V_m$  values characteristic of border control area were attained at higher depths. The data reported in Figure 7 showed that for retrievals #3, #7, #8, #9, #10, and #11, no significant differences were observed between the %  $V_m$  decreases within the first 20 and 40  $\mu\text{m}$ , and for these samples the  $V_m$  values characteristic of border control area were already attained at a 20  $\mu\text{m}$  depth.

Raman spectroscopy has been widely used to investigate the mechanism of tetragonal to monoclinic transformation. In general, the Mehl-Avrami-Johnson theory describes the phase transformation of solids at constant temperature [52]. According to this model, the dependence of  $V_m$  monoclinic content on the ageing time is expressed by the following equation [23,40,52]:

$$V_m = 1 - \left(1 - V_m^0\right)^{-(bt)^n} \quad (2)$$

where  $t$  is the ageing time,  $b$  is a parameter that depends on both growth and nucleation rates of monoclinic nuclei,  $V_m^0$  is the fraction of monoclinic phase in the material at the beginning of the ageing test, and  $n$  is an exponent that was found to range between 0.3 and 4.

The Mehl-Avrami-Johnson law has been typically used to describe the kinetics of crystallization, but it can also be applied to other phase changes of materials, like chemical reactions. According to previous studies, it has also been applied to retrievals [13,38].

Based on Equation (2), Figure 8a shows the plot of  $\ln(\ln(1 - V_m^0/1 - V_m))$  versus  $\ln(t)$ , where  $V_m$  and  $V_m^0$  were the average data obtained from the Raman spectra of the worn central region and unworn border area of each retrieval (measured under optical conditions (a)) and  $t$  is the follow-up. To achieve a higher reliability, the graph also contains data reported in our previous study, obtained under the same optical conditions [13].

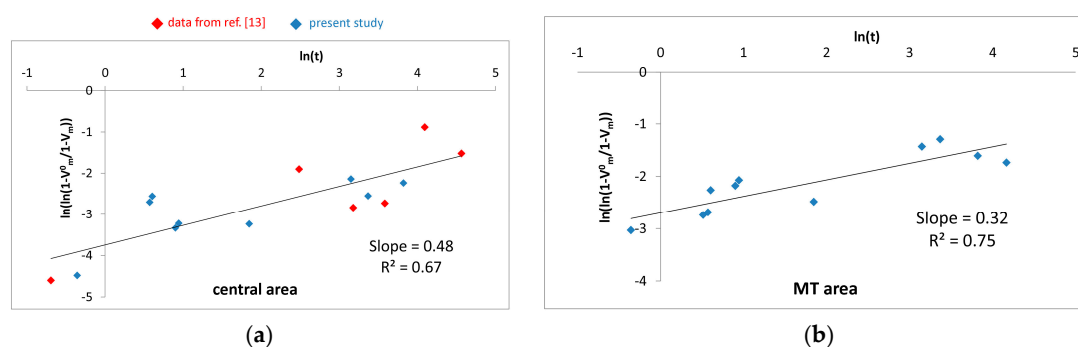


**Figure 8.** Plot of  $\ln(\ln(1 - V_m^0/1 - V_m))$  versus  $\ln(t)$ , where  $t$  is the follow-up,  $V_m^0$  is the average monoclinic content obtained from the Raman spectra of the unworn border area of the retrievals, and  $V_m$  is the average monoclinic content obtained from the Raman analysis (a) near the centre of the articulating surface using optical conditions (a) in the present study and in a previous one [13], and (b) near the MT region using optical conditions (b).

Figure 8b reports the corresponding plot obtained by using as  $V_m$  values those measured in the MT region of the retrievals analysed in the present study under optical conditions (b).

The  $n$  values, calculated as the slopes of the best regression lines corresponding to the experimental data obtained in the centre of the articulating surface and in the MT region, were found to be 0.48 and 0.32, respectively, i.e., below 1, as reported in our previous study [13].

A value of 1, according to the Mehl–Avrami–Johnson law [53], refers to nucleation only. A value between 3 and 4 indicates a nucleation and three-dimensional growth behaviour and was observed for unconstrained zirconia (Y-TZP), where no matrix prevents transformation [10]. On the contrary,  $n$  values close to 4 reveal that the main contribution to the kinetics of transformation comes from the growth of pre-existing monoclinic nuclei [7].

As previously observed by Deville et al. [10], values as low as those obtained in the present study suggest that the growth stage is absent and the nucleation stage is not occurring as freely as it would in unconstrained zirconia: the alumina matrix prevents the propagation of transformation and partially avoids nucleation of the monoclinic phase.

## 5. Conclusions

Eleven BioloX<sup>®</sup> delta femoral heads retrieved from patients after different periods (ranging between 0.1 and 5.4 years) were analysed in different areas, i.e., in their border, at the centre of the articulating surface and in the MT region. Although the number of the analysed retrievals was small, the results obtained allowed to gain more insights into the wear behaviour of BioloX<sup>®</sup> delta hip prostheses on a molecular scale.

The suitability of the border of the retrievals as a reliable control area for comparison was demonstrated; the in vivo permanence for 5.4 years was found to not alter the  $V_m$  monoclinic content in the border control area of BioloX<sup>®</sup> delta femoral heads. Both photoemission and Raman analyses confirmed, as already reported [13], that the manufacturer improved the material properties since the introduction of BioloX<sup>®</sup> delta into the market; however, batch-to-batch differences seem to be still present, in agreement with other studies [38,40].

Only for one retrieval (i.e., #2), stress related to MT appeared a more severe condition able to induce zirconia phase transformation. For all other retrievals, stresses related to loading in the central region and to MT phenomenon in the corresponding area were conducive to a zirconia phase transformation of nearly the same extent. For most retrievals, the phase transition in the MT area involved less than 20  $\mu\text{m}$ . With regards to photoemission measurements, the MT area behaved differently from the centre of the articulating surface in only two femoral heads, where micro-cracking was observed.

**Supplementary Materials:** The following figures are available online at [www.mdpi.com/1996-1944/10/7/744/s1](http://www.mdpi.com/1996-1944/10/7/744/s1), Figure S1: Average FWHM values (FWHM  $\pm$  standard deviation) of  $R_1$  and  $R_2$  bands obtained from the fitting of the emission spectra recorded under optical conditions (c) in different areas of the explanted BioloX<sup>®</sup> delta femoral heads. When present, different letters on the histogram bars indicate significant differences among the areas of each retrieval. Figure S2: Trend of the FWHM of  $R_1$  (a) and  $R_2$  (b) photoemission bands and  $V_m$  monoclinic zirconia content (c) measured in the border control areas of the retrievals as a function of the implantation year. Left: single retrievals data from the present study and reference [13]; right: average data from the present study and reference [13]. Figure S3: The trend of the %  $V_m$  increase observed in the centre and MT areas of the retrievals under study as a function of follow-up. The %  $V_m$  increase was calculated with respect to the control border of the same femoral head, under the same optical conditions (a) or (b). Figure S4:  $V_m$  values measured 100  $\mu\text{m}$  below the surface of retrievals #1, #2, #3, #5, #7, #8, #9, #10, #11 in depth profiling analyses and in their border control area under optical conditions (b).

**Acknowledgments:** The authors thank Barbara Bordini for the statistical analyses. This work was supported by the institutional academic RFO funds of Paola Taddei (University of Bologna).

**Author Contributions:** Saverio Affatato conceived the study and Paola Taddei designed the micro-Raman and photoemission experiments; Eleonora Pavoni and Paola Taddei performed the experiments; Paola Taddei and Eleonora Pavoni analysed the data; Saverio Affatato provided retrievals and related information; Eleonora Pavoni wrote the first draft; and Paola Taddei wrote the final paper and revised it.

**Conflicts of Interest:** The authors declare no conflict of interest. The founding sponsors had no role in the design of the study; in the collection, analyses, or interpretation of data; in the writing of the manuscript, and in the decision to publish the results.

## References

1. Burger, W.; Richter, H.G. High strength and toughness alumina matrix composites by transformation toughening and “in situ” platelet reinforcement (ZPTA)—The new generation of bioceramics. *Key Eng. Mater.* **2001**, *192–195*, 545–548. [[CrossRef](#)]
2. Bradt, R.C. Cr<sub>2</sub>O<sub>3</sub> Solid Solution Hardening of Al<sub>2</sub>O<sub>3</sub>. *J. Am. Ceram. Soc.* **1967**, *5*, 54–55. [[CrossRef](#)]
3. Magnani, G.; Brillante, A. Effect of the composition and sintering process on mechanical properties and residual stresses in zirconia alumina composites. *J. Eur. Ceram. Soc.* **2005**, *25*, 3383–3392. [[CrossRef](#)]
4. Willmann, G. Ceramics for total hip replacement—What a surgeon should know. *Orthopedics* **1998**, *21*, 173–180. [[PubMed](#)]
5. Willmann, G. The evolution of ceramics in total hip arthroplasty. *Hip Int.* **2000**, *10*, 193–203.
6. Ma, L.; Rainforth, W.M. A study of BioloX<sup>®</sup> delta subject to water lubricated reciprocating wear. *Tribol. Int.* **2010**, *43*, 1872–1881. [[CrossRef](#)]
7. Chevalier, J.; Cales, B.; Drouin, J.M. Low-temperature aging of Y-TZP ceramics. *J. Am. Ceram. Soc.* **1999**, *82*, 2150–2154. [[CrossRef](#)]
8. Chevalier, J. What future for zirconia as a biomaterial? *Biomaterials* **2006**, *27*, 535–543. [[CrossRef](#)] [[PubMed](#)]
9. Chevalier, J.; Gremillard, L.; Deville, S. Low-temperature degradation of zirconia and implications for biomedical implants. *Annu. Rev. Mater. Res.* **2007**, *37*, 1–32. [[CrossRef](#)]
10. Deville, S.; Chevalier, J.; Dauvergne, C.H.; Fantozzi, G.; Bartolomé, J.F.; Moya, S.; Torrecillas, R. Microstructural investigation of the aging behavior of (3Y-TZP)–Al<sub>2</sub>O<sub>3</sub> composites. *J. Am. Ceram. Soc.* **2005**, *88*, 1273–1280. [[CrossRef](#)]
11. Elpers, M.; Nam, D.; Boydston-White, S.; Ast, M.P.; Wright, T.M.; Padgett, D.E. Zirconia phase transformation, metal transfer, and surface roughness in retrieved ceramic composite femoral heads in total hip arthroplasty. *J. Arthroplasty* **2014**, *29*, 2219–2223. [[CrossRef](#)] [[PubMed](#)]
12. Lombardi, A.V.; Berend, K.R.; Seng, B.E.; Clarke, I.C.; Adams, J.B. Delta ceramic-on-alumina ceramic articulation in primary THA: Prospective, randomized FDA-IDE study and retrieval analysis. *Clin. Orthop. Relat. Res.* **2010**, *468*, 367–374. [[CrossRef](#)] [[PubMed](#)]
13. Taddei, P.; Modena, E.; Traina, F.; Affatato, S. Raman and fluorescence investigations on retrieved BioloX<sup>®</sup> delta femoral heads. *J. Raman Spectrosc.* **2012**, *43*, 1868–1876. [[CrossRef](#)]
14. Affatato, S.; Modena, E.; Toni, A.; Taddei, P. Retrieval analysis of three generations of BioloX<sup>®</sup> femoral heads: Spectroscopic and SEM characterization. *J. Mech. Behav. Biomed.* **2012**, *13*, 118–128. [[CrossRef](#)] [[PubMed](#)]
15. Affatato, S.; Ruggiero, A.; De Mattia, J.S.; Taddei, P. Does metal transfer affect the tribological behaviour of femoral heads? Roughness and phase transformation analyses on retrieved zirconia and BioloX<sup>®</sup> delta composites. *Compos. Part B-Eng.* **2016**, *92*, 290–298. [[CrossRef](#)]
16. Taddei, P.; Ruggiero, A.; Pavoni, E.; Affatato, S. Transfer of metallic debris after in vitro ceramic-on-metal simulation: Wear and degradation in BioloX<sup>®</sup> delta composite femoral heads. *Compos. Part B-Eng.* **2017**, *115*, 477–487. [[CrossRef](#)]
17. Chong, B.C.; Jeong, J.Y.; Won, S.S.; Deug, J.K.; Koo, K.H.; Kim, H.J. Transfer of metallic debris from the metal surface of an acetabular cup to artificial femoral heads by scraping: Comparison between alumina and cobalt-chrome heads. *J. Biomed. Mater. Res. B* **2008**, *85*, 204–209. [[CrossRef](#)] [[PubMed](#)]
18. Brandt, J.M.; Gascoyne, T.C.; Guenther, L.E.; Allen, A.; Hedden, D.R.; Turgeon, T.R.; Bohm, E.R. Clinical failure analysis of contemporary ceramic-on-ceramic total hip replacements. *Proc. Inst. Mech. Eng. Part H J. Eng. Med.* **2013**, *227*, 833–846. [[CrossRef](#)] [[PubMed](#)]
19. Müller, F.; Hagymási, M.; Greil, P.; Zeiler, G.; Schuh, A. Transfer of metallic debris after dislocation of ceramic femoral heads in hip prostheses. *Arch. Orthop. Trauma Surg.* **2006**, *126*, 174–180. [[CrossRef](#)] [[PubMed](#)]
20. Kim, Y.H.; Ritchie, A.; Hardaker, C. Surface roughness of ceramic femoral heads after in vivo transfer of metal: Correlation to polyethylene wear. *J. Bone Jt. Surg. Am.* **2005**, *87*, 577–582. [[CrossRef](#)]
21. Bal, B.S.; Rahaman, M.N.; Aleto, T.; Miller, F.S.; Traina, F.; Toni, A. The significance of metal staining on alumina femoral heads in total hip arthroplasty. *J. Arthroplasty* **2007**, *22*, 14–23. [[CrossRef](#)] [[PubMed](#)]
22. Katagiri, G.; Ishida, H.; Ishitani, A.; Masaki, T. *Science and Technology of Zirconia*; American Ceramic Society: Westerville, OH, USA, 1988; pp. 537–544.
23. Pezzotti, G.; Yamada, K.; Sakakura, S.; Pitto, R.P. Raman spectroscopic analysis of advanced ceramic composite for hip prosthesis. *J. Am. Ceram. Soc.* **2008**, *91*, 1199–1206. [[CrossRef](#)]

24. Clarke, D.R.; Adar, F. Measurement of the crystallographically transformed zone produced by fracture in ceramics containing tetragonal zirconia. *J. Am. Ceram. Soc.* **1982**, *65*, 284–288. [[CrossRef](#)]
25. Garcia, M.A.; Paje, S.E.; Llopis, J. Relationship between mechanical grinding and photoluminescence of zirconia-toughened-alumina ceramics. *Mater. Sci. Eng.* **2002**, *325*, 302–306. [[CrossRef](#)]
26. Ma, Q.; Clarke, D.R. Piezospectroscopic determination of residual stresses in polycrystalline alumina. *J. Am. Ceram. Soc.* **1994**, *77*, 298–302. [[CrossRef](#)]
27. He, J.; Clarke, D.R. Determination of the piezospectroscopic coefficients for chromium-doped sapphire. *J. Am. Ceram. Soc.* **1995**, *78*, 1347–1353. [[CrossRef](#)]
28. Krishnan, R.; Kesavamoorthy, R.; Dash, S.; Tyagi, A.K.; Raj, B. Raman spectroscopic and photoluminescence investigations on laser surface modified  $\alpha$ -Al<sub>2</sub>O<sub>3</sub> coatings. *Scr. Mater.* **2003**, *48*, 1099–1104. [[CrossRef](#)]
29. Sergo, V.; Pezzotti, G.; Sbaizero, O.; Nishida, T. Grain size influence on residual stresses in alumina/zirconia composites. *Acta Mater.* **1998**, *46*, 1701–1710. [[CrossRef](#)]
30. Grabner, L. Spectroscopic techniques for the measurement of residual stress in sintered Al<sub>2</sub>O<sub>3</sub>. *J. Appl. Phys.* **1978**, *49*, 580–583. [[CrossRef](#)]
31. Affatato, S.; Ruggiero, A.; Merola, M.; Logozzo, S. Does metal transfer differ on retrieved BioloX<sup>®</sup> Delta composites femoral heads? Surface investigation on three BioloX<sup>®</sup> generations from a biotribological point of view. *Compos. Part B-Eng.* **2017**, *113*, 164–173. [[CrossRef](#)]
32. Fagnano, C.; Rossi, M.; Porter, R.S.; Ottani, S. A study on solid-state drawn fibers of polyethylene by confocal Raman microspectrometry: Evaluation of the orientation profiles of amorphous and crystalline phases across the fiber section. *Polymer* **2001**, *42*, 5871–5883. [[CrossRef](#)]
33. Mc Lure, D.S. Optical Spectra of transition metal ions in corundum. *J. Phys. Chem.* **1962**, *36*, 2757–2779. [[CrossRef](#)]
34. Maiman, T.H. Stimulated optical radiation in ruby. *Nature* **1960**, *187*, 493–494. [[CrossRef](#)]
35. Philippi, C.M.; Mazdiyasi, K.S. Infrared and Raman spectra of zirconia polymorphs. *J. Am. Ceram. Soc.* **1971**, *54*, 254–258. [[CrossRef](#)]
36. Ishigame, M.; Sakurai, T. Temperature dependence of the Raman spectra of ZrO<sub>2</sub>. *J. Am. Ceram. Soc.* **1977**, *60*, 367–369. [[CrossRef](#)]
37. Porto, S.P.S.; Krishnan, R.S. Raman effect of corundum. *J. Chem. Phys.* **1967**, *47*, 1009–1012. [[CrossRef](#)]
38. Pezzotti, G.; Affatato, S.; Rondinella, A.; Yorifuji, M.; Marin, E.; Zhu, W.; McEntire, B.; Bal, S.B.; Yamamoto, K. In Vitro versus In Vivo Phase Instability of Zirconia-Toughened Alumina Femoral Heads: A Critical Comparative Assessment. *Materials* **2017**, *10*, 466. [[CrossRef](#)]
39. Insley, G.M.; Streicher, R.M. Next generation ceramic based on zirconia toughened alumina for hip joint prostheses. *Key Eng. Mater.* **2004**, *254*, 675–678. [[CrossRef](#)]
40. Chevalier, J.; Grandjean, S.; Kuntz, M.; Pezzotti, M. On the kinetics and impact of tetragonal to monoclinic transformation in an alumina/zirconia composite for arthroplasty applications. *Biomaterials* **2009**, *30*, 5279–5282. [[CrossRef](#)] [[PubMed](#)]
41. Bal, S.B.; Zhu, W.; Zanicco, M.; Marin, E.; Sugano, N.; McEntire, B.J.; Pezzotti, G. Reconciling in vivo and in vitro kinetics of the polymorphic transformation in zirconia-toughened alumina for hip joints: I. Phenomenology. *J. Mater. Sci. Eng. C* **2017**, *72*, 252–258. [[CrossRef](#)] [[PubMed](#)]
42. Taddei, P.; Affatato, S.; Fagnano, C.; Toni, A. Photoluminescence investigations on alumina ceramic bearing couples tested under different angles of inclination in a hip joint simulator. *J. Mater. Sci.* **2006**, *41*, 399–407. [[CrossRef](#)]
43. Taddei, P.; Affatato, S.; Torrecillas, R.; Fagnano, C.; Ferrieri, P.; Toni, A. Wear behaviour, fluorescence and SEM investigations on nanocomposite zirconia-toughened alumina. *J. Mater. Sci.* **2006**, *41*, 5310–5316. [[CrossRef](#)]
44. Chevalier, J.; Taddei, P.; Gremillard, L.; Deville, S.; Fantozzi, G.; Bartolomé, J.F.; Pecharroman, C.; Moya, J.S.; Diaz, L.A.; Torrecillas, R.; et al. Reliability assessment in advanced nanocomposite materials for orthopaedic applications. *J. Mech. Behav. Biomed. Mater.* **2011**, *4*, 303–314. [[CrossRef](#)] [[PubMed](#)]
45. Ma, Q.; Clarke, D.R. Stress measurements in single-crystal and polycrystalline ceramics using their optical fluorescence. *J. Am. Ceram. Soc.* **1993**, *76*, 1433–1440. [[CrossRef](#)]
46. Gregori, G.; Burger, W.; Sergo, V. Piezo-spectroscopy analysis of the residual stress in zirconia-toughened alumina ceramics: The influence of the tetragonal to monoclinic transformation. *Mater. Sci. Eng.* **1999**, *A271*, 401–406. [[CrossRef](#)]

47. Ortiz, M.; Suresh, S. Statistical properties of residual stresses and intergranular fracture in ceramic materials. *J. Appl. Mech.* **1993**, *60*, 77–84. [[CrossRef](#)]
48. Boffelli, M.; Doimo, A.; Marin, E.; Puppulin, L.; Zhu, W.; Sugano, N.; Clarke, I.C.; Pezzotti, G. Chemically driven tetragonal-to-monoclinic polymorphic transformation in retrieved ZTA femoral heads from dual mobility hip implants. *J. Mech. Behav. Biomed. Mater.* **2016**, *56*, 195–204. [[CrossRef](#)] [[PubMed](#)]
49. Pezzotti, G.; Porporati, A. Raman spectroscopic analysis of phase transformation and stress patterns in zirconia hip joints. *J. Biomed. Opt.* **2004**, *9*, 372–384. [[CrossRef](#)] [[PubMed](#)]
50. Parkes, M.; Sayer, K.; Goldhofer, M.; Cann, P.; Walter, W.L.; Jeffers, J. Zirconia phase transformation in retrieved, wear simulated and artificially aged ceramic femoral heads. *J. Orthop. Res.* **2017**. [[CrossRef](#)] [[PubMed](#)]
51. Zhu, W.; Pezzotti, G.; Boffelli, M.; Chotanaphuti, T.; Khuangsirikul, S.; Sugano, N. Chemistry-driven structural alterations in short-term retrieved ceramic-on-metal hip implants: Evidence for in vivo incompatibility between ceramic and metal counterparts. *J. Biomed. Mater. Res. Part B Appl. Biomater.* **2016**. [[CrossRef](#)] [[PubMed](#)]
52. Johnson, W.A.; Mehl, R.F. Reaction Kinetics in Processes of Nucleation and Growth. *Trans. Am. Inst. Min. Metall. Pet. Eng.* **1939**, *135*, 416–441.
53. Christian, J.W. *The Theory of Transformation in Metals and Alloys*; Pergamon Press: Oxford, UK, 1965; pp. 525–548.



© 2017 by the authors. Licensee MDPI, Basel, Switzerland. This article is an open access article distributed under the terms and conditions of the Creative Commons Attribution (CC BY) license (<http://creativecommons.org/licenses/by/4.0/>).